

Energy-Efficient Movable Antennas: Mechanical Power Modeling and Performance Optimization

Xin Wei, *Graduate Student Member, IEEE*, Weidong Mei, *Member, IEEE*, Xuan Huang, Zhi Chen, *Senior Member, IEEE*, and Boyu Ning, *Member, IEEE*

Abstract—Movable antennas (MAs) offer additional spatial degrees of freedom (DoFs) to enhance wireless communication performance through local antenna movement in a confined region. However, to achieve accurate and fast antenna movement, MA drivers entail non-negligible mechanical power consumption, rendering energy efficiency (EE) optimization more critical compared to conventional fixed-position antenna (FPA) systems. To address this problem, we develop in this paper a fundamental power consumption model for stepper motor-driven multi-MA systems by resorting to basic electric motor theory. Based on this model, we investigate an EE maximization problem for the downlink transmission from a multi-MA base station (BS) to multiple single-antenna users. In particular, we aim to jointly optimize the MAs' positions and moving speeds as well as the BS's transmit precoding matrix subject to collision-avoidance constraints during the multi-MA movements. However, this problem appears to be difficult to be solved optimally. To tackle this challenge, we first reveal that the collision-avoidance constraints can always be relaxed without loss of optimality by properly renumbering the MA indices. For the resulting relaxed problem, we first consider a simplified single-user setup and uncover a hidden monotonicity of the EE performance with respect to the MAs' moving speeds. To solve the remaining optimization problem, we develop a two-layer optimization framework. In the inner layer, the Dinkelbach algorithm is employed to derive the optimal beamforming solution in a semi-closed form for any given MA positions. In the outer layer, a sequential update algorithm is proposed to iteratively refine the MA positions based on the optimal values obtained from the inner layer. Next, we proceed to the general multi-user case and propose an alternating optimization (AO) algorithm to obtain a high-quality suboptimal solution. Numerical results demonstrate that despite the additional mechanical power consumption, the proposed algorithms can outperform both conventional FPA systems and existing EE maximization algorithms that neglect mechanical power consumption.

Index Terms—Movable antennas, energy efficiency, stepper motor, mechanical power model, moving speed, alternating optimization, sequential update.

I. INTRODUCTION

Driven by the growing demand for higher data rates, lower latency, and greater reliability in future sixth-generation (6G) wireless networks, communication system design is increasingly evolving toward architectures that emphasize spectral

This paper will be presented in part at the IEEE Global Communications Conference (GLOBECOM), Taipei, Taiwan, 2025 [1].

Xin Wei, Weidong Mei, Zhi Chen, and Boyu Ning are with the National Key Laboratory of Wireless Communications, University of Electronic Science and Technology of China, Chengdu 611731, China (e-mail: xinwei@std.uestc.edu.cn, wmei@uestc.edu.cn, chenzhi@uestc.edu.cn, boyding@outlook.com).

Xuan Huang is with the School of Information and Communication Engineering, University of Electronic Science and Technology of China, Chengdu 611731, China (e-mail: huang.xuan@std.uestc.edu.cn).

efficiency, spatial intelligence, and configurational flexibility. Technologies such as massive multiple-input multiple-output (MIMO) [2] and extremely large antenna arrays (ELAAs) [3] have shown strong potential in exploiting spatial degrees of freedom (DoFs) to achieve significant gains in throughput, interference suppression, and dynamic beamforming. However, these techniques largely rely on fixed-position antennas (FPAs), whose static geometric configurations result in fixed spatial correlations, thus significantly limiting their adaptability to dynamic environments and leading to suboptimal performance [4], [5].

To address the limitations of FPA architectures, movable antenna (MA) systems (also known as fluid antenna systems [6]) have recently emerged as a promising solution by introducing reconfigurable array geometries [7]. Specifically, compared to FPAs, MAs can reposition their elements, either individually or array-wise, by using mechanical actuators or electrically controlled mechanisms within a predefined local region [8], [9]. This spatial reconfigurability allows the antenna geometry to dynamically adapt to real-time channel conditions and user locations, thus offering new DoFs for performance enhancement. The promising benefits of MA systems have spurred great enthusiasm in investigating MA position optimization in various wireless systems. For example, the authors in [10] investigated the MA-aided point-to-point MIMO systems and demonstrated that antenna position optimization can significantly enhance MIMO channel capacity by increasing both spatial channel power gains and spatial multiplexing gain. Beyond rate improvement, MAs have also been leveraged to manipulate the spatial correlations among steering vectors, thereby achieving more flexible beam nulling [11], multi-beam forming [12], [13], and wide-beam coverage [14]. Furthermore, MA position optimization has been explored in other scenarios such as secure communications [15]–[17], single- and multi-user multiple-input single-output (MISO) [18]–[20], cognitive radio [21], relaying systems [22], non-orthogonal multiple access (NOMA) [23], [24], intelligent reflecting surface (IRS)-aided wireless communications [25], [26], wireless sensing or integrated sensing and communications (ISAC) [27]–[30], among others. To further advance the frontier of reconfigurable antenna technologies, novel architectures such as six-dimensional movable antenna (6DMA) [31] and pinching antenna systems [32] have also been proposed recently.

However, despite these prior works, the energy efficiency (EE) of MA systems has not been thoroughly investigated. Particularly, enabling precise position adjustment and motion of MAs typically relies on mechanical actuators (e.g., stepper motors), which can incur non-negligible additional energy

consumption. Furthermore, antenna repositioning inevitably incurs a finite movement delay and potential inter-MA collision, reducing the effective duration available for wireless data transmission. Considering these practical factors, it remains unclear whether MAs can still outperform FPAs in terms of EE. To answer this question, a handful of recent works have investigated the EE performance optimization for MA systems [33]–[35]. Specifically, the authors in [33] studied the EE maximization for an MA-MIMO system based on statistical channel state information (CSI). However, their analysis considers only the power consumption from data transmission, while ignoring the mechanical energy consumed by antenna movement, which can be substantial in practice. Although the authors in [34] incorporate the energy consumption of MA movement into the EE analysis, it models the mechanical power consumption as a fixed constant, overlooking its dependency on motion dynamics such as displacement and speed, and thus lacks a detailed power consumption model for the MA drivers. Recently, a parallel work [35] proposed an energy consumption model for mechanically-driven MA systems. However, it focuses solely on a single MA at the user side, without theoretically characterizing the impact of antenna velocity on the EE performance or accounting for potential inter-MA collisions in multi-MA movement.

Motivated by above, this paper investigates a more general and challenging EE maximization problem for a mechanically-driven MA system, where a base station (BS) equipped with a linear MA array transmits to multiple single-FPA users at the same time, as shown in Fig. 1. The main contributions of this paper are summarized as follows:

- 1) First, we develop an overall power consumption model for the considered mechanically-driven multi-MA systems based on the basic electric motor theory, which accounts for both the mechanical energy consumed by MA drivers and the electrical energy consumed by data transmission. Building on this model, we formulate an EE (i.e., the ratio of the sum rate of all users to the above energy consumption) maximization problem by jointly optimizing the MAs' destination positions and moving speeds as well as the BS's transmit precoding matrix, subject to the collision-avoidance constraints during the multi-MA movements. Although this problem is non-convex and difficult to be optimally solved, we first show that the collision-avoidance constraints can always be relaxed without loss of optimality by properly renumbering the MA indices, thus greatly simplifying the optimization problem.
- 2) Next, to solve the resulting relaxed EE maximization problem, we start from the single-user case and reveal a hidden monotonicity of the EE performance with respect to (w.r.t.) the MAs' moving speeds. For the remaining joint BS beamforming and MA position optimization, we recast this problem into a two-layer formulation. In the inner layer, the Dinkelbach algorithm is applied to derive the optimal transmit beamforming in a semi-closed form for any given MA positions. Whereas in the outer layer, the sequential update algorithm is adopted to iteratively optimize the MA positions based on the optimal transmit beamforming derived in the inner layer.

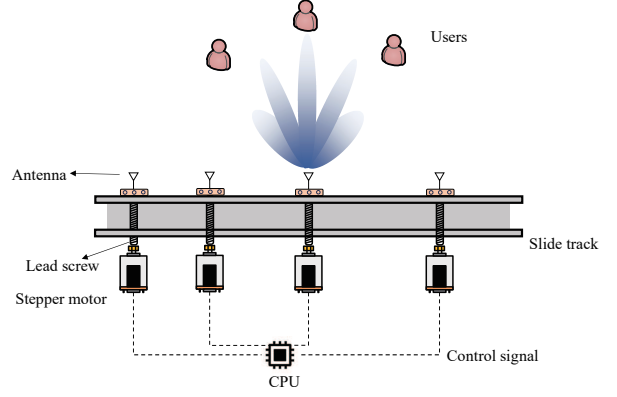


Fig. 1: Stepper motor-driven MA system with multiple users.

- 3) For the general multi-user case, we propose an alternating optimization (AO) algorithm that alternately optimizes the BS precoding and MA positions using the successive convex approximation (SCA) and sequential update methods, respectively. Finally, simulation results demonstrate that our proposed algorithms consistently outperform both conventional FPA-based systems and existing EE maximization schemes that ignore mechanical power consumption, under both single-user and multi-user setups. It is also shown that the optimized MA positions by our proposed algorithm achieve a superior balance between rate improvement via antenna movement and the associated mechanical power consumption compared to other baseline schemes.

The rest of this paper is organized as follows. Section II presents the overall power consumption model for our considered mechanically-driven MA system and formulates the EE maximization problem. Sections III and IV present our proposed solutions to this problem in the single- and multi-user cases, respectively. Section V presents the numerical results. Finally, Section VI concludes this paper and discusses future directions.

Notations: a , \mathbf{a} , \mathbf{A} , and \mathcal{A} denote a scalar, a vector, a matrix and a set, respectively. For a complex number a , $\angle a$, $|a|$, and a^* denote its phase, amplitude and conjugate, respectively. $(\cdot)^T$, $(\cdot)^H$, and $(\cdot)^{-1}$ denote the transpose, conjugate transpose and inverse of a matrix, respectively. \mathbb{R} and \mathbb{C} denote the sets of real numbers and complex numbers, respectively. $|a|$ and $\|a\|_2$ denote the amplitude of a scalar a and the norm of a vector a , respectively. $\mathbf{A}[n, :]$ and $\mathbf{A}[:, m]$ denotes the n -th row and the m -th column of a matrix \mathbf{A} , respectively. $\text{sign}(a)$ is the sign function which is given by $\text{sign}(a) \triangleq \begin{cases} \frac{a}{|a|}, & a \neq 0 \\ 0, & a = 0 \end{cases}$.

II. SYSTEM MODEL AND PROBLEM FORMULATION

A. System Model

As shown in Fig. 1, we consider an MA-enhanced communication system where a BS equipped with N MAs serves K users each with a single FPA. We consider that the positions of the N MAs can be flexibly adjusted within a linear array with the length of A meters (m). Each MA is assumed to be mechanically driven via a dedicated stepper motor, which employs a lead screw with an outer radius of l_0 as its linear

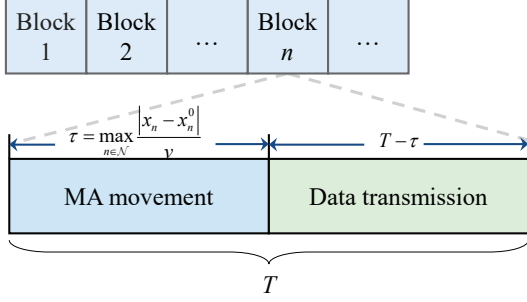


Fig. 2: Two-stage transmission protocol in mechanically-driven MA systems.

actuator. Considering the discrete nature of stepper motors which rotate by a fixed step angle, the MAs can only move in a discrete step size rather than continuously. Let ω_D denote the step angle of the stepper motor. Then, the corresponding step size of each MA is expressed as $d_s = \omega_D l_0$. As a result, the continuous linear array is discretized into $M = \lfloor \frac{A}{d_s} \rfloor$ points as the MAs' candidate positions, where $\lfloor \cdot \rfloor$ denotes the round-down operation. Let $\mathcal{C}_t \triangleq \{0, d_s, 2d_s, \dots, (M-1)d_s\}$ denote the set of all candidate positions and $x_n^0, x_n \in \mathcal{C}_t$ denote the initial position of the n -th MA, $n \in \mathcal{N} \triangleq \{1, 2, \dots, N\}$. Define $\mathbf{x}^0 \triangleq [x_1^0, x_2^0, \dots, x_N^0]^T \in \mathbb{R}^{N \times 1}$ as the current position vector (CPV) of all MAs. Without loss of generality, we assume $x_1^0 < x_2^0 < \dots < x_N^0$.

We assume a block-fading channel model and focus on a given time block of duration T , which is divided into two stages, as illustrated in Fig. 2. Specifically, in the first stage, each stepper motor drives its associated MA to its destination position. We assume that the BS remains nearly inactive in this phase with negligible energy consumption; hence, the power consumption in this stage is mainly from the stepper motors. Let $x_n \in \mathcal{C}_t$, $n \in \mathcal{N}$ denote the destination position of the n -th MA and $\mathbf{x} = [x_1, x_2, \dots, x_N]^T \in \mathbb{R}^{N \times 1}$ denote the destination positions vector (DPV) of all MAs. To reduce the modeling and controlling complexity, we assume that all MAs move at the same constant speed, denoted by v . As such, the delay for the n -th MA to move from its current position to the destination position is given by

$$\tau_n \triangleq \frac{|x_n - x_n^0|}{v}, \quad \forall n \in \mathcal{N}. \quad (1)$$

Moreover, to avoid mutual coupling among all MAs, we set

$$|x_i - x_j| \geq D_{\min}, \quad \forall i, j \in \mathcal{N}, i \neq j, \quad (2)$$

where D_{\min} is the minimum inter-antenna spacing to avoid mutual coupling.

The first stage ends after all MAs reach their associated destination positions. Hence, the actual time delay in antenna movement is given by

$$\tau \triangleq \max_{n \in \mathcal{N}} \tau_n. \quad (3)$$

To ensure that the antenna movement can be finished within the channel coherence time, it must hold that $\tau < T$, or equivalently,

$$v \geq \max_{n \in \mathcal{N}} \frac{|x_n - x_n^0|}{T}. \quad (4)$$

It is also worth noting that there may exist inter-MA

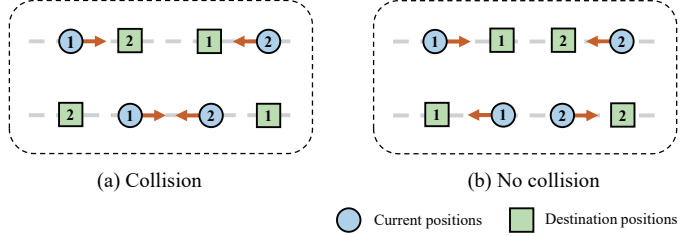


Fig. 3: Illustration of multi-MA movements with $N = 2$.

collisions in moving the MAs from their current positions to the destination positions, as illustrated in Fig. 3(a). To prevent such collisions, the distance between any two distinct MAs must remain greater than a prescribed threshold, denoted by D_{th} (with $D_{\text{th}} \geq D_{\min}$), at all times during the movement. Specifically, given the current and destination positions of the n -th MA, i.e., x_n^0 and x_n , its position at any time instant within the movement period is given by

$$s_n(t) \triangleq \begin{cases} x_n^0 + vt \cdot \text{sign}(x_n - x_n^0), & 0 \leq t < \tau_n, \\ x_n, & \tau_n \leq t \leq \tau. \end{cases} \quad (5)$$

Consequently, the collision-avoidance constraint is given by

$$|s_i(t) - s_j(t)| \geq D_{\text{th}}, \quad \forall i, j \in \mathcal{N}, i \neq j, \quad t \in [0, \tau]. \quad (6)$$

B. Power Consumption Model

The total power consumption of the considered MA system comprises the energy consumed by the MA drivers in the first stage and that radiated for data transmission in the second stage, i.e.,¹

$$E_{\text{total}}(\mathbf{W}, \mathbf{x}, v) = \underbrace{\sum_{n=1}^N \tau_n P_M(v)}_{\text{First stage}} + \underbrace{(T - \tau) P_D(\mathbf{W})}_{\text{Second stage}}, \quad (7)$$

where $P_M(v)$ and $P_D(\mathbf{W})$ denote the power consumption for the MA driver and data transmission, respectively. The matrix $\mathbf{W} \triangleq [\mathbf{w}_1, \mathbf{w}_2, \dots, \mathbf{w}_K] \in \mathbb{C}^{N \times K}$ represents the transmit precoding matrix for the K users with $\mathbf{w}_k \in \mathbb{C}^{N \times 1}$ denoting the transmit beamforming vector for the k -th user. For the power consumption model during data transmission, it primarily includes the radiated power used for signal transmission and the static circuit power consumption, which is given by [36]

$$P_D(\mathbf{W}) = \text{Tr}(\mathbf{W}\mathbf{W}^H) + P_s, \quad (8)$$

where $\text{Tr}(\mathbf{W}\mathbf{W}^H)$ denotes the BS's transmit power, and P_s denotes the static circuit power consumption.

Next, we develop the power consumption model of the MA drivers. According to basic electric motor theory, the power consumption of the stepper motor primarily results from the mechanical work required to drive the load, which depends on the MA's moving speed v and is given by [37]

$$P_M(v) = \omega M(\omega) = \frac{v}{l_0} M \left(\frac{v}{l_0} \right), \quad (9)$$

¹For simplicity, we assume that all stepper motors are identical and share the same torque-speed characteristics. Nevertheless, the proposed power consumption model remains applicable to scenarios where different stepper motors with varying characteristics are employed.

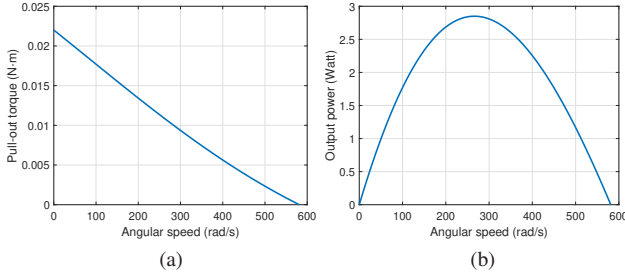


Fig. 4: (a) Pull-out torque; (b) Output power versus the angular speed of the stepper motor.

where $\omega = v/l_0$ denotes the angular velocity of the stepper motor associated with each MA. In addition, $M(\omega)$ represents the pull-out torque of the stepper motor and is characterized as [37]

$$M(\omega) = \frac{p\psi_M V}{\sqrt{R^2 + \omega^2 L^2}} - \frac{p\omega\psi_M^2 R}{R^2 + \omega^2 L^2}, \quad (10)$$

where p denotes the number of the rotor teeth, ψ_M denotes the peak magnet flux linking each winding, V denotes the voltage, R denotes the phase resistance, and L denotes the phase inductance.

To facilitate a deeper understanding of the mechanical power consumption, we consider a simplified case where a single stepper motor drives a single MA, and plot in Figs. 4(a) and 4(b) the pull-out torque in (10) and the power consumption in (9) versus the speed of its driven load, i.e., v , respectively. The voltage is $V = 11.94$ volt (V), the phase resistance is $R = 75$ Ohm (Ω), the phase inductance is $L = 65.6$ millihenry (mH), the number of rotor teeth is $p = 6$, the peak magnet flux linking each winding is $\psi_M = 0.023$ Weber (Wb), and the radius of the lead screw is $l_0 = 5$ millimeter (mm).

It is observed from Fig. 4(a) that the pull-out torque of the stepper motor gradually decreases with its angular velocity ω_n . This is because the pull-out torque produced by a stepper motor is proportional to the current through the coils. As ω_n increases, the back electromotive force (EMF) generated by the motor's windings increases, which acts against the applied voltage and reduces the effective voltage driving the current through the motor coils. On the other hand, stepper motors are inductive loads. The inductive resistance of the coils also increases with ω_n , which limits the current that can be supplied to the windings. Hence, it is shown in Fig. 4(b) that the power consumption of a stepper motor first increases with v , achieving its maximum value, and then decreases, rather than remaining constant. It is also worth noting that the power consumption drops to zero when the angular speed reaches its maximum value (denoted by ω_M), corresponding to the no-load condition, which is typically unachievable in practice due to the non-negligible weight of the MA. Therefore, we set a maximum achievable angular speed ω_{\max} , $\omega_{\max} < \omega_M$ for the stepper motor in this paper, accounting for the load of the MA. As such, the maximum moving speed of the MA is given by $v_{\max} = \omega_{\max} l_0$.

C. Problem Formulation

Based on (6)-(10), we formulate an EE maximization problem for the considered MA system in this subsection. Let $\mathbf{h}_k(\mathbf{x}) \triangleq [h_k(x_1), h_k(x_2), \dots, h_k(x_n)] \in \mathbb{C}^{N \times 1}$ denote the

BS-user k channel w.r.t. DPV \mathbf{x} . Then, the received signal-to-interference-and-noise ratio (SINR) at user k is given by

$$\gamma_k(\mathbf{W}, \mathbf{x}) = \frac{|\mathbf{h}_k^H(\mathbf{x}) \mathbf{w}_k|^2}{\sum_{i \neq k}^K |\mathbf{h}_k^H(\mathbf{x}) \mathbf{w}_i|^2 + \sigma^2}, \quad \forall k \in \mathcal{K}. \quad (11)$$

Accordingly, the achievable rate of user k is given by

$$R_k(\mathbf{W}, \mathbf{x}) = \log_2(1 + \gamma_k(\mathbf{W}, \mathbf{x})), \quad (12)$$

where σ^2 denotes the average noise power at each user. As such, the energy efficiency of the considered multi-MA system within a channel coherence block can be expressed as

$$\text{EE}(\mathbf{W}, \mathbf{x}, v) = \frac{(T - \tau) \sum_{k=1}^K R_k(\mathbf{W}, \mathbf{x})}{E_{\text{total}}(\mathbf{W}, \mathbf{x}, v)}. \quad (13)$$

It is observed from (13) that the EE performance depends on the speed of the MA, v . As v increases, the movement delay τ will decrease, which helps increase the achievable rate in the numerator of (13). However, it remains unclear whether the total power consumption in the denominator of (13) will increase or not. As such, there exists a non-trivial relationship between the EE in (13) and the MA's speed v . Furthermore, the EE in (13) also depends on the DPV \mathbf{x} , as it affects both the communication channel quality and the movement delay for a given v . Last but not least, the BS's transmit precoding matrix \mathbf{W} can also affect (13) by increasing the achievable rates of the users via beamforming optimization.

Hence, in this paper, we aim to maximize (13) by jointly optimizing the DPV \mathbf{x} , the BS's transmit precoding matrix \mathbf{W} , and the moving speed of the MA v . The associated optimization problem can be formulated as²

$$(P1) \quad \max_{\mathbf{W}, \mathbf{x}, v} \text{EE}(\mathbf{x}, \mathbf{W}, v)$$

$$\text{s.t.} \quad \text{Tr}(\mathbf{W}\mathbf{W}^H) \leq P_{\max}, \quad (14a)$$

$$x_n \in \mathcal{C}_t, \quad \forall n \in \mathcal{N}, \quad (14b)$$

$$\max_{n \in \mathcal{N}} \frac{|x_n - x_n^0|}{T} \leq v \leq v_{\max}. \quad (14c)$$

$$(2), (6).$$

Note that for (P1), if the optimized DPV \mathbf{x} is set identical to the CPV, i.e., $x_n = x_n^0, \forall n \in \mathcal{N}$, the MA system reduces to the conventional FPA system. As such, the optimal EE value of (P1) is ensured to be no worse than that by an FPA system. Moreover, if the channel coherence time T is sufficiently large, e.g., $T \rightarrow \infty$, the EE in (13) will degrade to conventional EE without accounting for the mechanical power consumption, i.e.,

$$\text{EE}(\mathbf{W}, \mathbf{x}, v) = \frac{\sum_{k=1}^K R_k(\mathbf{W}, \mathbf{x})}{\text{Tr}(\mathbf{W}\mathbf{W}^H) + P_s}, \quad (15)$$

as studied in [33] and [34]. It follows that a different DPV from that in [33] and [34] is generally needed considering the mechanical power consumption, especially if the channel coherence time is not long.

²Note that to characterize the fundamental limit of the energy efficiency of the considered MA system, we assume that all required channel state information is available via the existing channel estimation techniques for MA systems; see [38]–[40].

However, (P1) is difficult to be solved optimally due to the collision-free constraints in (6), the fractional form of the objective function, and the nonlinear and intricate expression of $P_M(v)$. Fortunately, it can be shown that we can safely drop (6) without loss of optimality of (P1), as presented in the following Proposition.

Proposition 1: For any given DPV \mathbf{x} , if the constraints in (6) are not satisfied, it can always be renumbered (jointly with the precoding matrix \mathbf{W}) to satisfy (6), without degrading the achieved EE performance.

Proof: See Appendix A. \blacksquare

Proposition 1 indicates that it suffices to solve (P1) without accounting for (6), denoted as (P1-relax), followed by an additional renumbering step. As illustrated in Fig. 3(b), if we renumber the two destination positions, then inter-MA collision can be avoided, and each MA's movement distance or time can be shortened as well. However, (P1-relax) is still a non-convex optimization problem due to its fractional objective function involving complex mechanical power consumption. In the next section, we first consider a simpler single-user scenario.

III. SINGLE-USER SCENARIO

In the single-user scenario, the EE performance in (13) can be simplified as

$$\begin{aligned} \text{EE}_{\text{SU}}(\mathbf{x}, \mathbf{w}, v) &= \frac{R(\mathbf{w}, \mathbf{x})}{E_{\text{total}}(\mathbf{w}, \mathbf{x}, v)} \\ &= \frac{(T - \tau) \log_2 \left(1 + |\mathbf{w}^H \mathbf{h}(\mathbf{x})|^2 / \sigma^2 \right)}{(T - \tau) \left(\|\mathbf{w}\|_2^2 + P_s \right) + P_M(v) \sum_{n=1}^N \tau_n}, \end{aligned} \quad (16)$$

where $\mathbf{w} \in \mathbb{C}^{N \times 1}$ denotes the transmit beamforming at the BS with $\|\mathbf{w}\|_2^2 \leq P_{\max}$, and the subscripts “ k ” in $R(\mathbf{w}, \mathbf{x})$ and \mathbf{w} are omitted in the single-user scenario without ambiguity. As such, (P1-relax) reduces to the following problem:

$$\begin{aligned} (\text{P2}) \quad &\max_{\mathbf{w}, \mathbf{x}, v} \text{EE}_{\text{SU}}(\mathbf{x}, \mathbf{w}, v) \\ \text{s.t.} \quad &\|\mathbf{w}\|_2^2 \leq P_{\max}, \\ &(2), (14b). \end{aligned} \quad (17a)$$

However, (P2) is still non-convex and challenging to be solved optimally. To address this, we reveal the hidden monotonicity of the EE performance w.r.t. the MA's moving speed first.

A. Optimal Moving Velocity

To cope with the highly nonlinear expression of $P_M(v)$ w.r.t. v , we introduce the following proposition to capture the relationship between EE and MA moving speed.

Proposition 2: For any given feasible DPV \mathbf{x} and the BS's transmit beamforming \mathbf{w} , the EE in (16) monotonically increases with v .

Proof: First, we recast the EE in (16) as a more tractable form:

$$\begin{aligned} \text{EE}_{\text{SU}}(v) &= \frac{(T - \tau) \log_2 \left(1 + |\mathbf{w}^H \mathbf{h}(\mathbf{x})|^2 / \sigma^2 \right)}{(T - \tau) \left(\|\mathbf{w}\|_2^2 + P_s \right) + P_M(v) \sum_{n=1}^N \tau_n}, \\ &= \frac{(vT - \Delta x) \log_2 \left(1 + |\mathbf{w}^H \mathbf{h}(\mathbf{x})|^2 / \sigma^2 \right)}{(vT - \Delta x) \left(\|\mathbf{w}\|_2^2 + P_s \right) + P_M(v) \sum_{n=1}^N |x_n - x_n^0|}, \end{aligned}$$

$$= \frac{\log_2 \left(1 + |\mathbf{w}^H \mathbf{h}(\mathbf{x})|^2 / \sigma^2 \right)}{\|\mathbf{w}\|_2^2 + P_s + f(v) \sum_{n=1}^N |x_n - x_n^0|}, \quad (18)$$

where $\Delta x \triangleq \max_{n \in \mathcal{N}} |x_n - x_n^0|$ and $f(v) \triangleq \frac{P_M(v)}{vT - \Delta x}$, respectively. It is evident that EE increases with v if $f(v)$ decreases with v . The first-order derivative of $f(v)$ is given by

$$\frac{\partial f(v)}{\partial v} = \frac{v \frac{\partial M(\omega)}{\partial \omega} (vT - \Delta x) - l_0 M \left(\frac{v}{l_0} \right) \Delta x}{l_0^2 (vT - \Delta x)^2}. \quad (19)$$

Note that $vT - \Delta x > 0$ due to the constraints in (4). Moreover, for practical stepper motors, its pull-out torque decreases with its angular velocity, as depicted in Fig. 4(a). Hence, we have $\frac{\partial M(\omega)}{\partial \omega} < 0$. Therefore, we can conclude that $\frac{\partial f(v)}{\partial v} < 0$, i.e., $f(v)$ monotonically decreases with v . This completes the proof. \blacksquare

Proposition 2 indicates that to maximize the EE of the considered mechanically-driven MA system in the single-user scenario, the stepper motor should always operate at its maximum speed, i.e., $v = v_{\max}$, which also helps prolong the time for data transmission. Then, by substituting $v = v_{\max}$ into (P2), (P2) can be simplified as

$$\begin{aligned} (\text{P3}) \quad &\max_{\mathbf{w}, \mathbf{x}} \text{EE}_{\text{SU}}(\mathbf{w}, \mathbf{x}, v_{\max}) \\ \text{s.t.} \quad &\frac{|x_n - x_n^0|}{T} \leq v_{\max}, \forall n \in \mathcal{N}, \\ &(2), (14b), (17a). \end{aligned} \quad (20a)$$

B. Proposed Algorithm for (P3)

However, (P3) is still difficult to be optimally solved. In the following, we propose a two-layer optimization algorithm to decompose it into two simpler subproblems. The inner problem optimizes the transmit beamforming vector \mathbf{w} with a given DPV \mathbf{x} , while the outer problem optimizes the DPV \mathbf{x} based on the optimal value of the inner problem. The inner and outer problems are respectively given by

$$(\text{P3-1}) \quad \max_{\mathbf{w}} \text{EE}_{\text{SU}}(\mathbf{w}, \mathbf{x}, v_{\max}), \quad \text{s.t.} \quad (17a).$$

and

$$(\text{P3-2}) \quad \max_{\mathbf{x}} \text{EE}_{\text{SU}}(\mathbf{w}(\mathbf{x}), \mathbf{x}, v_{\max}) \quad \text{s.t.} \quad (2), (14b), (20a),$$

where $\mathbf{w}(\mathbf{x})$ denotes the optimal solution to (P3-1). In the following, we elaborate on the approaches for solving these two subproblems.

1) *Inner-Layer Optimization:* To solve (P3-1), we first rewrite \mathbf{w} into the following form:

$$\mathbf{w} = \sqrt{p} \mathbf{w}_0, \quad (21)$$

where p denotes the BS's transmit power with $0 \leq p \leq P_{\max}$ and \mathbf{w}_0 denotes the normalized transmit beamforming vector with $\|\mathbf{w}_0\|_2^2 = 1$. By substituting (21) into the objective function of (P3-1), it can be observed that for any given transmit power p , the transmit beamforming vector \mathbf{w}_0 should be set as the maximum-ratio transmission (MRT) based on $\mathbf{h}(\mathbf{x})$, i.e.,

$$\mathbf{w}_0^* (\mathbf{x}) = \frac{\mathbf{h}(\mathbf{x})}{\|\mathbf{h}(\mathbf{x})\|_2}. \quad (22)$$

With (21) and (22), we can simplify the expression of EE in (P3-1) and recast it as a power control problem, i.e.,

$$(P3-1) \max_{0 \leq p \leq P_{\max}} \text{EE}_{\text{SU}}(p) = \frac{a \log_2(1 + p \|\mathbf{h}(\mathbf{x})\|_2^2 / \sigma^2)}{ap + b},$$

where $a \triangleq T - \tau$ and $b \triangleq aP_s + P_M(v_{\max}) \sum_{n=1}^N \tau_n$, respectively. Note that (P3-1) is a classical fractional programming (FP) problem, for which the Dinkelbach's algorithm can be employed. Specifically, in the l -th iteration of the Dinkelbach's algorithm, (P3-1) is transformed into the following subtractive form, i.e.,

$$(P3-1-l) \max_{0 \leq p \leq P_{\max}} f^{(l)}(p),$$

where

$$f^{(l)} \triangleq a \log_2(1 + p \|\mathbf{h}(\mathbf{x})\|_2^2 / \sigma^2) - \eta^{(l-1)}(ap + b) \quad (23)$$

and

$$\eta^{(l-1)} \triangleq \frac{a \log_2(1 + p^{(l-1)} \|\mathbf{h}(\mathbf{x})\|_2^2 / \sigma^2)}{ap^{(l-1)} + b} \quad (24)$$

denotes the EE value obtained in the $(l-1)$ -th Dinkelbach iteration with $p^{(l-1)}$ denoting the optimal transmit power obtained in this iteration. Note that $f^{(l)}(p)$ is a concave function in p . Hence, by setting $\frac{\partial f^{(l)}(p)}{\partial p} = 0$, the optimal transmit power that maximizes (23) can be obtained as

$$p^{(l)}(\mathbf{x}) = \min \left(\left[\hat{p}^{(l)}(\mathbf{x}) \right]^+, P_{\max} \right), \quad (25)$$

where $\hat{p}^{(l)}(\mathbf{x})$ is given by

$$\hat{p}^{(l)}(\mathbf{x}) = \frac{1}{\eta^{(l-1)} \ln 2} - \frac{\sigma^2}{\|\mathbf{h}(\mathbf{x})\|_2^2}, \quad (26)$$

and $[z]^+ = \max(z, 0)$. Based on (24) and (25), we can compute the value of $\eta^{(l)}$ and proceed to the $(l+1)$ -th Dinkelbach iteration. It can be shown that $\eta^{(l)}$ monotonically increases with the iteration and converges to an optimal solution to (P3-1) [36]. Let $p^*(\mathbf{x})$ denote the optimal transmit power obtained by the Dinkelbach algorithm. Then, the optimal transmit beamforming vector \mathbf{w}^* for (P3-1) can be expressed as

$$\mathbf{w}^*(\mathbf{x}) = \sqrt{p^*(\mathbf{x})} \mathbf{w}_0^*(\mathbf{x}) = \sqrt{p^*(\mathbf{x})} \frac{\mathbf{h}(\mathbf{x})}{\|\mathbf{h}(\mathbf{x})\|_2}. \quad (27)$$

The overall procedures of the proposed algorithm to solve (P3-1) are summarized in Algorithm 1.

2) *Outer-Layer Optimization*: By employing Algorithm 1, we can obtain the optimal value of (P3-1) with any given DPV \mathbf{x} . As such, (P3-2) can be simplified as

$$(P3-2) \max_{\mathbf{x}} \text{EE}_{\text{SU}}(\mathbf{w}^*(\mathbf{x}), \mathbf{x}, v_{\max}) \quad \text{s.t. (2), (14b), (20a)}$$

where $\mathbf{w}^*(\mathbf{x})$ is the optimal transmit beamforming vector given in (27). Due to the discrete step size of the MA, we can adopt the sequential update algorithm proposed in [25] to solve (P3-2) efficiently. Notably, such a sequential update algorithm has also been utilized in many existing works for antenna position optimization with an intractable objective function [21], [28] even for continuous antenna movements. Compared to the gradient-based algorithms, the sequential update algorithm is

Algorithm 1 Proposed Algorithm for Solving (P3-1)

- 1: Initialize $p^{(0)} = 0$ and the convergence accuracy ϵ .
 - 2: Set $l = 1$.
 - 3: Initialize $\eta^{(l-1)}$ according to (24).
 - 4: **repeat**
 - 5: Set $l = l + 1$.
 - 6: Calculate $p^{(l)}$ according to (25).
 - 7: Calculate $\eta^{(l)}$ according to (24).
 - 8: **until** $|\eta^{(l)} - \eta^{(l-1)}| < \epsilon$.
 - 9: Set $p^* = p^{(l)}$.
 - 10: Output \mathbf{w}^* with p^* according to (27) as the optimized solutions to (P3-1).
-

applicable to any problem structure and dispenses with the need for complex gradient calculation. Whereas compared to the heuristic antenna position optimization algorithms such as particle swarm optimization (PSO) [41], the sequential update algorithm ensures local optimality and leads to a lower computational complexity, as will also be demonstrated in Section V via simulation.

Specifically, we sequentially update the position of each MA over multiple rounds, each including N iterations. In the n -th iteration, we only optimize the position of the n -th MA (i.e., x_n), while keeping the positions of the other $(N-1)$ MAs fixed. Let us consider the n -th iteration in the r -th round and denote by $x_j^{(r)}$ the updated position of the j -th MA in this round, $1 \leq j \leq n-1$. Then, the set of all feasible destination positions for optimizing x_n is given by

$$\mathcal{X}_n^{(r)} = \left\{ x \mid x \in \mathcal{C}_t, \left| x - x_j^{(r)} \right| \geq D_{\min}, \forall 1 \leq j \leq n-1, \right. \\ \left. \left| x - x_j^{(r-1)} \right| \geq D_{\min}, \forall n+1 \leq j \leq N, \right. \\ \left. \left| x - x_n^0 \right| \leq v_{\max} T \right\}, \quad 1 < n < N. \quad (28)$$

In addition, we set $\mathcal{X}_1^{(r)} = \{x \mid x \in \mathcal{C}_t, |x - x_j^{(r-1)}| \geq D_{\min}, \forall 2 \leq j \leq N, |x - x_1^0| \leq v_{\max} T\}$ and $\mathcal{X}_N^{(r)} = \{x \mid x \in \mathcal{C}_t, |x - x_j^{(r)}| \geq D_{\min}, \forall 1 \leq j \leq N-1, |x - x_N^0| \leq v_{\max} T\}$. Let $\hat{\mathbf{x}} = [x_1^{(r)}, \dots, x_{n-1}^{(r)}, x_n, x_{n+1}^{(r)}, \dots, x_N^{(r)}]^T$. Then, we can optimize x_n as

$$x_n^{(r)} = \arg \max_{x_n \in \mathcal{X}_n^{(r)}} \text{EE}_{\text{SU}}(\mathbf{w}^*(\hat{\mathbf{x}}), \hat{\mathbf{x}}, v_{\max}), \quad (29)$$

which can be optimally solved via an enumeration within $\mathcal{X}_n^{(r)}$. Next, we can proceed to update the position of the $(n+1)$ -th MA in this round.

Let $\mathbf{x}^* = [x_1^*, x_2^*, \dots, x_N^*]^T$ denote the optimized DPV by the multi-round sequential update. The corresponding optimal transmit beamforming vector can be obtained as $\mathbf{w}^*(\mathbf{x}^*) = \sqrt{p^*(\mathbf{x}^*)} \frac{\mathbf{h}(\mathbf{x}^*)}{\|\mathbf{h}(\mathbf{x}^*)\|_2}$. Finally, to ensure that the optimized DPV satisfies the constraints in (6) as presented in the proof of Proposition 1, we sort the destination positions in an ascending order as $x_{q_1}^* < x_{q_2}^* < \dots < x_{q_N}^*$, with permutation indices $q_n \in \mathcal{N}$. Then, we set $x_n^* = x_{q_n}^*$ and $w_n^* = w_{q_n}^*$, $n \in \mathcal{N}$, where w_n^* denotes the n -th entry of $\mathbf{w}^*(\mathbf{x}^*)$.

The overall algorithm for solving (P3-2) is summarized in Algorithm 2. Since each iteration yields a non-decreasing value of (P3-2), the convergence of the proposed two-layer op-

Algorithm 2 Proposed Algorithm for Solving (P3-2)

- 1: Initialize $x_n^{(0)}$, $\forall n \in \mathcal{N}$ and the convergence accuracy ϵ .
- 2: Set $r = 0$.
- 3: Calculate $\text{EE}_{\text{SU}}^{(r)}$ with $x_n = x_n^{(0)}$, $\forall n \in \mathcal{N}$ according to (16).
- 4: **repeat**
- 5: Set $r = r + 1$.
- 6: **for** $n = 1 \rightarrow N$ **do**
- 7: Construct $\mathcal{X}_n^{(r)}$ according to (28).
- 8: Update $x_n^{(r)}$ via (29).
- 9: Set $n = n + 1$.
- 10: **end for**
- 11: **until** the fractional increase of the objective value of (P3-3) is below the given threshold ϵ .
- 12: Set $\mathbf{x}^* = [x_1^*, x_2^*, \dots, x_N^*]^T$, with $x_n^* = x_n^{(r)}$, $n \in \mathcal{N}$.
- 13: Calculate $\mathbf{w}^*(\mathbf{x}^*) = [w_1^*, w_2^*, \dots, w_N^*]^T$ via (27).
- 14: Sort \mathbf{x}^* in an ascending order as $x_{q_1}^* < x_{q_2}^* < \dots < x_{q_N}^*$.
- 15: Set $x_n^* = x_{q_n}^*$ and $w_n^* = w_{q_n}^*$, $\forall n \in \mathcal{N}$.
- 16: Output $\mathbf{w}^*(\mathbf{x}^*)$ and \mathbf{x}^* as the optimized solutions to (P3-2).

timization framework is guaranteed. The computational complexity for Algorithm 2 is given by $\mathcal{O}(I_w I_x NM)$, where I_w denotes the number of iterations of the Dinkelbach algorithm in solving (P3-1), and I_x denotes the number of sequential update rounds in solving (P3-2).

IV. MULTI-USER SCENARIO

In this section, we focus on the general multi-user scenario, i.e., (P1-relax). First, we show that the optimal MA moving velocity is still v_{\max} in the multi-user scenario. To this end, we rewrite the EE in (13) into the following form:

$$\begin{aligned} \text{EE}(\mathbf{W}, \mathbf{x}, v) &= \frac{(T - \tau) \sum_{k=1}^K R_k(\mathbf{W}, \mathbf{x})}{\sum_{n=1}^N \tau_n P_M(v) + (T - \tau) P_D(\mathbf{W})} \\ &= \frac{\sum_{k=1}^K R_k(\mathbf{W}, \mathbf{x})}{f(v) \sum_{n=1}^N |x_n - x_n^0| + P_D(\mathbf{W})}, \end{aligned} \quad (30)$$

where $f(v) = \frac{P_M(v)}{vT - \Delta x}$ and $\Delta x = \max_{n \in \mathcal{N}} |x_n - x_n^0|$. shown in the proof of Proposition 2, $f(v)$ decreases with v . Hence, the EE in (30) in the multi-user scenario also increases with v , and (P1-relax) can be simplified as

$$(P4) \quad \max_{\mathbf{W}, \mathbf{x}} \text{EE}(\mathbf{W}, \mathbf{x}, v_{\max}) \quad \text{s.t. (2), (14a), (14b), (20a),}$$

by setting $v = v_{\max}$. However, (P4) remains difficult to solve due to the strong coupling between the design variables \mathbf{W} and \mathbf{x} . To address this difficulty, we develop an AO algorithm to alternately optimize these variables.

A. Proposed AO Algorithm for (P4)

1) *Optimizing \mathbf{W} with Given \mathbf{x} :* First, we optimize the transmit precoding matrix \mathbf{W} with any given DPV \mathbf{x} . Under this condition, (P4) can be simplified as

$$(P4-1) \quad \max_{\mathbf{W}} \text{EE}(\mathbf{W}, \mathbf{x}, v_{\max}) \quad \text{s.t. (14a).}$$

Similar to the single-user setup, we apply the Dinkelbach's algorithm to deal with the fractional programming problem. Specifically, in the l -th iteration of the Dinkelbach's algorithm, (P4-1) is transformed into the following subtractive form:

$$(P4-1-l) \quad \max_{\mathbf{W}} g^{(l)}(\mathbf{W}) \quad \text{s.t. (14a),}$$

where

$$g^{(l)}(\mathbf{W}) \triangleq a \sum_{k=1}^K R_k(\mathbf{W}, \mathbf{x}) - \eta^{(l-1)} (a \text{Tr}(\mathbf{W} \mathbf{W}^H) + b) \quad (31)$$

and

$$\eta^{(l-1)} \triangleq \frac{a \sum_{k=1}^K R_k(\mathbf{W}^{(l-1)}, \mathbf{x})}{a \text{Tr}(\mathbf{W}^{(l-1)} (\mathbf{W}^{(l-1)})^H) + b} \quad (32)$$

and $\mathbf{W}^{(l-1)}$ denotes the optimized transmit beamforming matrix in $(l-1)$ -th iteration. However, (P4-1-l) is still non-convex due to the complicated expression of $R_k(\mathbf{W}, \mathbf{x})$. To proceed, we introduce a slack variable $\chi = [\chi_1, \chi_2, \dots, \chi_K]$ for the SINR term inside $R_k(\mathbf{W}, \mathbf{x})$, i.e., $\gamma_k(\mathbf{W}, \mathbf{x})$, and transform (P4-1-l) into

$$\begin{aligned} (P4-1-l) \quad &\max_{\mathbf{W}, \chi} \bar{g}^{(l)}(\mathbf{W}, \chi) \\ &\text{s.t. } \gamma_k(\mathbf{W}, \mathbf{x}) \geq \chi_k, \forall k \in \mathcal{K}, \end{aligned} \quad (33a)$$

where

$$\begin{aligned} \bar{g}^{(l)}(\mathbf{W}, \chi) &\triangleq a \sum_{k=1}^K \log_2(1 + \chi_k) \\ &\quad - \eta^{(l-1)} (a \text{Tr}(\mathbf{W} \mathbf{W}^H) + b). \end{aligned} \quad (34)$$

To handle the non-convex constraints in (33a), we introduce another positive slack variable $\xi = [\xi_1, \xi_2, \dots, \xi_K]$ and reformulate (33a) into an equivalent form:

$$\left| \mathbf{h}_k^H(\mathbf{x}) \mathbf{w}_k \right|^2 \geq \xi_k \chi_k, \quad \forall k, \quad (35)$$

and

$$\sum_{i \neq k}^K \left| \mathbf{h}_k^H(\mathbf{x}) \mathbf{w}_i \right|^2 + \sigma^2 \leq \xi_k, \quad \forall k. \quad (36)$$

It can be observed that (36) is convex while (35) still remains non-convex. Nonetheless, the term $\mathbf{h}_k^H(\mathbf{x}) \mathbf{w}_k$ in constraints (35) can be expressed as a real number through an arbitrary rotation to the beamforming vector \mathbf{w}_k . As a result, (35) is equivalent to $\Re(\mathbf{h}_k^H(\mathbf{x}) \mathbf{w}_k) \geq \sqrt{\xi_k \chi_k}$. As such, by replacing the concave term $\sqrt{\xi_k \chi_k}$ with its first-order Taylor expansion at given feasible points $\{\chi_k^{(t-1)}\}_{k=1}^K$ and $\{\xi_k^{(t-1)}\}_{k=1}^K$, the constraints in (35) can be expressed as

$$\begin{aligned} \Re(\mathbf{h}_k^H(\mathbf{x}) \mathbf{w}_k) &\geq \sqrt{\xi_k^{(t-1)} \chi_k^{(t-1)}} + \frac{1}{2} \sqrt{\frac{\chi_k^{(t-1)}}{\xi_k^{(t-1)}}} (\xi_k - \xi_k^{(t-1)}) \\ &\quad + \frac{1}{2} \sqrt{\frac{\xi_k^{(t-1)}}{\chi_k^{(t-1)}}} (\chi_k - \chi_k^{(t-1)}), \quad \forall k. \end{aligned} \quad (37)$$

Algorithm 3 Proposed Algorithm for Solving (P4-1)

- 1: Initialize $\mathbf{W}^{(0)}$ and the convergence accuracy ϵ_1 .
- 2: Set $l = 0$.
- 3: Initialize $\eta^{(l-1)}$ according to (32).
- 4: **repeat**
- 5: Set $l = l + 1$.
- 6: Initialize $\chi^{(0)}$, $\xi^{(0)}$, and convergence accuracy ϵ_2 .
- 7: Set $t = 1$.
- 8: **repeat**
- 9: Solve (P4-1-l-t) with given $\chi^{(t-1)}$ and $\xi^{(t-1)}$ via the interior-point method.
- 10: **until** the fractional increase of the objective value of (P4-1-l-t) is below the given threshold ϵ_2 .
- 11: Output $\mathbf{W}^{(l)}$ as the solution to (P4-1-l).
- 12: Calculate $\eta^{(l)}$ according to (32).
- 13: **until** $|\eta^{(l)} - \eta^{(l-1)}| \geq \epsilon_1$
- 14: Output $\mathbf{W}^{(l)}$ as the optimized solutions to (P4-1).

Based on the above approximations, (P4-1-l-t) can be formulated approximated as the following problem

$$\begin{aligned}
 \text{(P4-1-l-t)} \quad & \max_{\mathbf{W}, \mathbf{x}, \xi} \bar{g}^{(l)}(\mathbf{W}, \mathbf{x}) \\
 \text{s.t.} \quad & (14a), (36), (37), \\
 & \xi_k > 0, \forall k \in \mathcal{K},
 \end{aligned} \tag{38a}$$

which is convex and can be efficiently solved by the interior-point method. The overall algorithm to solve (P4-1) is summarized in Algorithm 3.

2) *Optimizing \mathbf{x} with Given \mathbf{W}* : Next, we optimize the DPV \mathbf{x} with any given transmit precoding matrix \mathbf{W} , which is equivalent to solve the following problem:

$$\text{(P4-2)} \quad \max_{\mathbf{x}} \text{EE}(\mathbf{W}, \mathbf{x}, v_{\max}) \quad \text{s.t. (2), (14b), (20a).}$$

Notably, (P4-2) shares a similar structure to (P3-2), differing primarily in the objective function. Therefore, the multi-round sequential update algorithm used to solve (P3-2) can also be applied here, by changing the objective function in (P3-2) to $\text{EE}(\mathbf{W}, \mathbf{x}, v_{\max})$ with a given transmit precoding matrix \mathbf{W} . For brevity, the details are omitted.

Let $\mathbf{x}^* = [x_1^*, x_2^*, \dots, x_N^*]^T$ denote the optimized (but unsorted) DPV obtained by the above process in each AO iteration. Similar to the single-user scenario, we sort \mathbf{x}^* in an ascending order as $x_{q_1}^* < x_{q_2}^* < \dots < x_{q_N}^*$ and set $x_n^* = x_{q_n}^*$, thereby avoiding inter-antenna collisions. In addition, the optimized transmit precoding matrix in Section IV-A1 should be updated as well, i.e., $\mathbf{W}[n, :] = \mathbf{W}[q_n, :]$, where $\mathbf{W}[n, :]$ denotes the n -th row of \mathbf{W} .

3) *Overall Algorithm*: Based on the above, we can alternately solve (P4-1) and (P4-2) via Algorithms 3 and 2, respectively. The overall algorithm to solve (P4) is summarized in Algorithm 4. Note that each iteration of the SCA procedure in Algorithm 3 produces a non-decreasing objective value, ensuring that (P4-1) converges to its maximum. Similarly, Algorithm 2 yields a non-decreasing objective value of (P4-2). Hence, the overall convergence of Algorithm 4 is guaranteed.

Finally, we analyze the computational complexity of Algorithm 4. According to [42], the computational complexity

Algorithm 4 Proposed Algorithm for Solving (P4)

- 1: Initialize $\mathbf{W}^{(0)}$, $\mathbf{x}^{(0)}$, the convergence accuracy ϵ .
- 2: Calculate the EE performance $\text{EE}^{(0)}$ with $\mathbf{W}^{(0)}$ and $\mathbf{x}^{(0)}$.
- 3: Set $l = 0$.
- 4: **repeat**
- 5: Set $l = l + 1$.
- 6: Obtain $\mathbf{W}^{(l)}$ with given $\mathbf{x}^{(l-1)}$ according to Algorithm 3.
- 7: Obtain $\mathbf{x}^{(l)}$ with given $\mathbf{W}^{(l)}$ via a similar process to Algorithm 2.
- 8: Sort $\mathbf{x}^{(l)}$ in an ascending order as $x_{q_1}^{(l)} < x_{q_2}^{(l)} < \dots < x_{q_N}^{(l)}$.
- 9: Update $x_n^{(l)} = x_{q_n}^{(l)}$ and $\mathbf{W}^{(l)}[n, :] = \mathbf{W}^{(l)}[q_n, :]$, $n \in \mathcal{N}$.
- 10: Calculate the EE performance $\text{EE}^{(l)}$ with $\mathbf{W}^{(l)}$ and $\mathbf{x}^{(l)}$.
- 11: **until** $|\text{EE}^{(l)} - \text{EE}^{(l-1)}| \leq \epsilon$
- 12: Output $\mathbf{W}^{(l)}$ and $\mathbf{x}^{(l)}$ as the optimized solutions to (P4).

for solving (P4-1) is given by $\mathcal{O}(I_w N^6 K^{1.5})$. In addition, the computational complexity for solving (P4-2) is given by $\mathcal{O}(I_x N M)$. As a result, the total complexity of Algorithm 4 is given by $\mathcal{O}(I_w N^6 K^{1.5} + I_x N M)$.

V. NUMERICAL RESULTS

In this section, we present numerical results to validate the efficacy of our proposed algorithms. Unless otherwise specified, the simulation parameters are set as follows. The carrier wavelength is $\lambda = 0.06$ meter (m). The length of the linear array is $A = 6\lambda = 0.36$ m. The initial positions of the N MAs are symmetrically distributed along the center of \mathcal{C}_t with a half-wavelength spacing. The number of MAs is $N = 6$, and that of users is $K = 2$. The BS's static circuit power consumption is $P_s = 30$ dBm, and its maximum transmit power is $P_{\max} = 30$ dBm. The time duration of a channel coherence block is $T = 0.25$ s. We consider the field-response-based channel model presented in [7] for MAs in the simulation. The distance from the BS to each user is uniformly distributed between 20 m and 100 m, and the path-loss exponent for the BS-user channels is $\alpha = 2.8$. The number of multipath components in the BS-user channels is $L = 10$, and their path gains are assumed to follow the circle symmetric complex Gaussian (CSCG) distribution, i.e., $g_{k,l} \sim \mathcal{CN}(0, \rho d_k^{-\alpha}/L)$, $l = 1, 2, \dots, L$, $k \in \mathcal{K}$, where ρ represents the path loss at the reference distance of 1 m. The angles of departure (AoDs) for these paths are assumed to be independent and identically distributed variables following the uniform distribution within $[-\frac{\pi}{2}, \frac{\pi}{2}]$. The average noise power is $\sigma^2 = -80$ dBm. Moreover, we consider the AM2224 high-speed stepper motor in this simulation [43], with the same parameters as those adopted in Fig. 4. The maximum angular speed of the stepper motor is $\omega_{\max} = 552$ rad/s. The step angle and radius of the lead screw is $\omega_D = \frac{\pi}{12}$ rad/s and $l_0 = 5$ mm, respectively. Hence, the step size of the stepper motor is $d_s = \omega_D l_0 \approx 1.2$ mm. All the results are averaged over 1000 independent channel realizations.

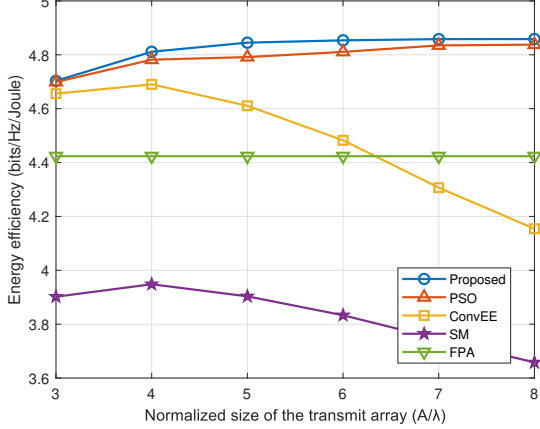


Fig. 5: EE performance versus the normalized size of transmit array.

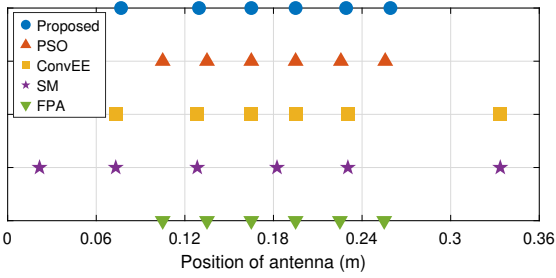


Fig. 6: Optimized positions of the MAs by different schemes.

Furthermore, we consider the following benchmark schemes for performance comparison:

- 1) **Benchmark 1: PSO.** In this benchmark, the DPV \mathbf{x} is optimized via the PSO method in the continuous space [41] and then quantized based on the step size d_s , and the transmit precoding matrix \mathbf{W} is optimized via a similar process as proposed in this paper.
- 2) **Benchmark 2: Conventional EE optimization (ConvEE).** The optimization problem (P1) is first solved by neglecting the mechanical power consumption, i.e., $P_m = 0$, via our proposed algorithms. Then, the actual EE performance involving the mechanical power consumption is calculated with the optimized MA positions and transmit precoding.
- 3) **Benchmark 3: Sum-rate maximization (SM).** In this benchmark, the transmit precoding matrix \mathbf{W} and DPV \mathbf{x} are optimized to solely maximize the achievable sum-rate $\sum_{k=1}^K R_k(\mathbf{W}, \mathbf{x})$. The transmit precoding matrix is optimized via the weighted minimum mean square error (WMMSE) algorithm with a fixed DPV \mathbf{x} [44]; while the DPV \mathbf{x} is optimized via the sequential update method presented in Algorithm 2.
- 4) **Benchmark 4: FPA.** In this benchmark, the DPV is fixed as $x_n = x_n^0$, and the BS's transmit precoding matrix is optimized via the Dinkelbach's algorithm.

A. Single-User System

First, we consider the single-user scenario and plot in Fig. 5 the EE performance versus the normalized size of the transmit array (i.e., A/λ). It is observed that the EE

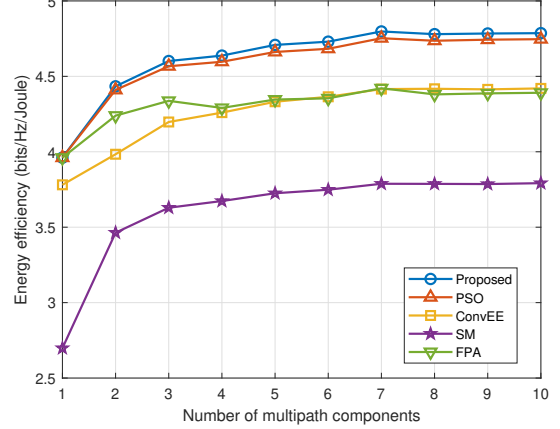


Fig. 7: EE performance versus the number of multipath components.

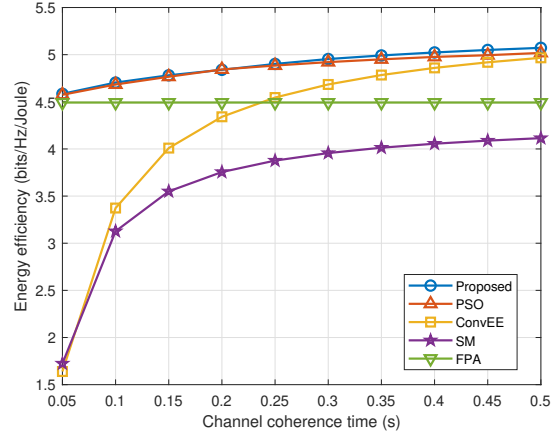


Fig. 8: EE performance versus the channel coherence time.

performance of our proposed algorithm increases with the size of \mathcal{C}_t and outperforms the PSO algorithm and other benchmarks. In contrast, the ConvEE benchmark exhibits a decline in EE performance as the size of \mathcal{C}_t increases, due to its omission of mechanical power consumption in optimization. As a result, the optimized DPV leads to longer movement distances from their associated CPV, thus degrading the EE performance. This highlights the necessity of accounting for mechanical power consumption in mechanically-driven MA systems. Furthermore, the EE performance of the SM benchmark is observed to be significantly worse compared to the other schemes. This behavior results from its exclusive focus on rate maximization while disregarding both mechanical and transmit power consumption, leading to substantial overall power consumption and degraded EE performance.

To gain more insights, we plot in Fig. 6 the optimized positions of the MAs by different schemes in one specific channel realization, with $N = 6$ and $A = 6\lambda$. It is observed that the optimized MA positions by the proposed algorithm are located closer to the initial positions (i.e., those of the FPA scheme) compared to those by the ConvEE and SM benchmarks, thereby reducing the mechanical energy consumption and movement delay due to the long-distance movement. In contrast, the optimized positions by the PSO algorithm are observed to be even closer to the initial antenna positions compared to the proposed algorithm. Although this proximity

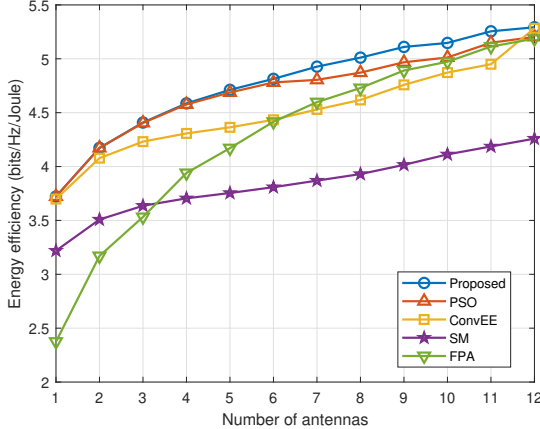


Fig. 9: EE performance versus the number of antennas.

helps reduce the mechanical power consumption, it also leads to less effective exploitation of the spatial diversity within the movement region. It follows that the proposed algorithm yields a better balance between the rate performance and power consumption than the other benchmark schemes.

Next, we plot in Fig. 7 the EE performance versus the number of multipath components in the BS-user channel (i.e., L). It is observed that the EE performance of all schemes (except the FPA benchmark) improves as the number of paths increases. This is because when L increases, the channel power gain within the movable region exhibits more significant fluctuation, resulting in enhanced spatial diversity gain. This helps shorten the movement time to identify the optimal antenna position that balances rate performance and energy consumption. In addition, the EE performance of all schemes except the SM benchmark is observed to be identical for $L = 1$. This is because under the MRT beamforming strategy in (22), the channel power gain $||\mathbf{h}(\mathbf{x})||^2$ becomes constant and independent of antenna position. It is also observed that the ConvEE and SM benchmarks yield the worst EE performance among all considered schemes, as similarly observed from previous figures.

Fig. 8 depicts the EE performance versus the channel coherence time T with $N = 6$. It is observed that the EE performance of all schemes (except the FPA benchmark) improves with increasing T , as this increases each MA's maximum allowable moving distance as seen from (4). Hence, more favorable antenna positions can be explored to improve the rate-energy trade-off. In contrast, the EE performance of the FPA benchmark keeps constant as T increases. Furthermore, it is observed that the improvement in the EE performance by the proposed scheme decreases with T and ultimately converges. This is because as T is sufficiently large, the EE in (13) will degrade to the conventional EE presented in (15), which is regardless of T , as discussed at the end of Section II. This also results in decreased performance gap between the proposed algorithm and the ConvEE benchmark as T increases.

Lastly, we plot in Fig. 9 the EE performance versus the number of antennas (i.e., N). It is observed that the EE performance of all considered schemes monotonically increases with N . On one hand, this is due to the improved beamforming gain by increasing N . On the other hand, this is due to

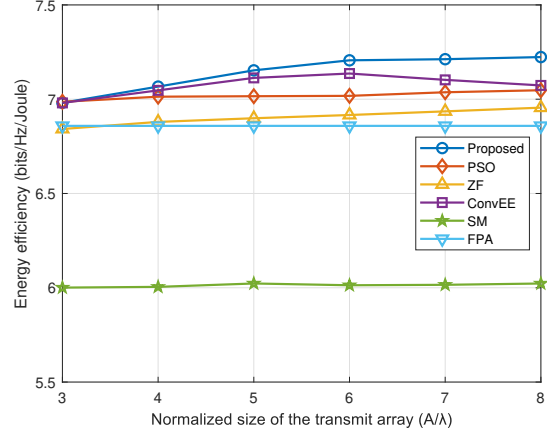


Fig. 10: EE performance versus the normalized size of the transmit region.

the reduced movement distance for each MA to cover as N increases considering the finite region size. It is also observed that the performance gaps between the proposed algorithm and the FPA and ConvEE benchmarks reduce as N increases. This is because there exists a maximum allowable number of MAs given the distance constraints in (2), i.e., $N_{\max} = A/D_{\min} = 12$. Thus, when N approaches 12, the flexibility of the antenna position optimization reduces, thus resulting in less performance gains from antenna movement.

B. Multi-User System

In this subsection, we present the simulation results for the multi-user scenario. Besides the baseline schemes adopted in the single-user scenario, we include a benchmark based on zero-forcing (ZF) precoding, where \mathbf{W} is fixed as the ZF precoder. The resulting power allocation and DPV \mathbf{x} can be optimized in a two-layer manner similarly to Algorithm 2. Specifically, in the inner layer, the power allocation is optimized via the Dinkelbach algorithm for any given \mathbf{x} [45]. In the outer layer, the DPV \mathbf{x} is optimized via the sequential update algorithm as in Section III-B2. This benchmark is marked as “ZF” in the subsequent figures.

First, we plot in Fig. 10 the EE performance versus the normalized size of the transmit array, i.e., A/λ . It is observed that the proposed algorithm consistently outperforms all benchmark schemes, while the ZF benchmark slightly outperforms the FPA benchmark. Moreover, compared with the single-user scenario, the EE improvement by increasing A is less significant in the multi-user setting. This is primarily due to the fact that the optimized MA positions at the BS need to cater for the channels for all users, thus resulting in less performance gain in sum rate and EE. Nonetheless, when $A = 8\lambda$, the proposed algorithm can still achieve an approximately 0.5 bps/Hz/Joule improvement over the FPA benchmark. It is also observed that both our proposed algorithm and the ZF benchmark can ensure a monotonic increase in EE as A increases. In contrast, the EE performance of the ConvEE benchmark degrades as $A \geq 6\lambda$, while that of the SM benchmark keeps almost constant and remains the worst among all considered schemes. This highlights the importance of balancing the data rate and mechanical energy consumption in the multi-user scenario as well.

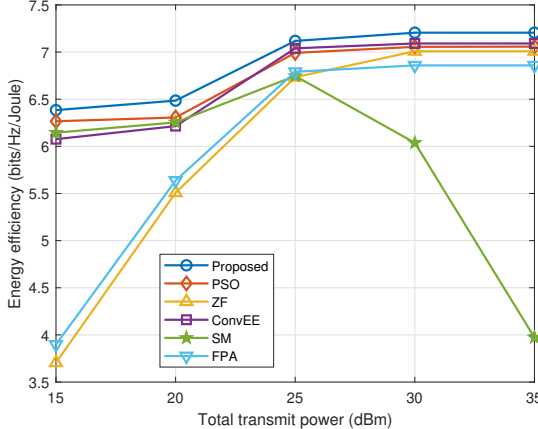


Fig. 11: EE performance versus the maximum transmit power.

Next, we plot in Fig. 11 the EE performance versus the maximum transmit power P_{\max} in the multi-user scenario. It is observed that the EE performance of all considered schemes improves with P_{\max} when $P_{\max} \leq 25$ dBm. This is because the EE performance is more dominated by the achievable rate in the low transmit power regime, compared to the total power consumption. Hence, all schemes should transmit at the maximum power to maximize the achievable rate. It is also interesting to note that unlike conventional EE maximization, there still exists certain performance gap (around 0.4 bps/Hz/Joule) between the proposed algorithm and SM benchmark in the low transmit power regime. This is because the additional mechanical power consumption also contributes to the EE performance, and the SM benchmark may introduce more significant mechanical power consumption compared to the proposed method. In addition, a significant performance gap between the proposed method and the FPA benchmark is observed in the low transmit power regime, implying that the rate gain from antenna movement can be dominant over the resulting mechanical power consumption for EE maximization in this regime. The ZF benchmark is observed to achieve an even worse performance than FPA as $P_{\max} \leq 15$ dBm. This is because, in the low-power regime, the received SINR of each user is primarily limited by the noise power σ^2 instead of inter-user interference. Consequently, the ZF benchmark, which focuses on interference suppression, may offer limited benefits.

On the other hand, when $P_{\max} > 25$ dBm, the total power consumption plays a more significant role. As a result, transmitting at the maximum power may result in a significant loss in EE, as observed from the SM benchmark. In contrast, the performance of other schemes is observed to remain constant as P_{\max} increases, suggesting that their transmit powers are unchanged to maximize the EE. Furthermore, the ZF benchmark is observed to achieve a close performance to the proposed method in the high transmit power regime, due to the more prominent effects of inter-user interference on the EE performance.

In Fig. 12, we plot the EE performance versus the channel coherence time (i.e., T). Similar to the observations made from Fig. 12, the EE performance by all schemes increases with T , and our proposed algorithm achieves the highest EE

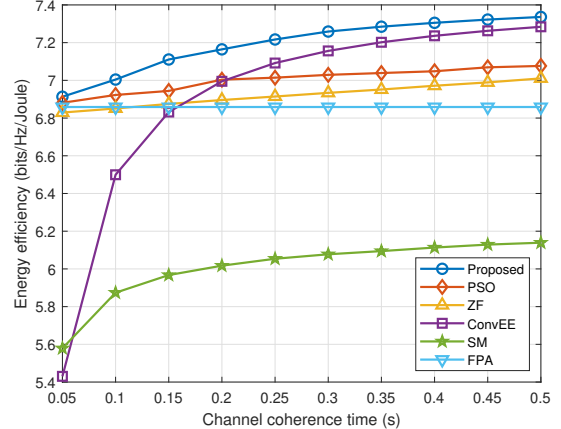


Fig. 12: EE performance versus the channel coherence time.

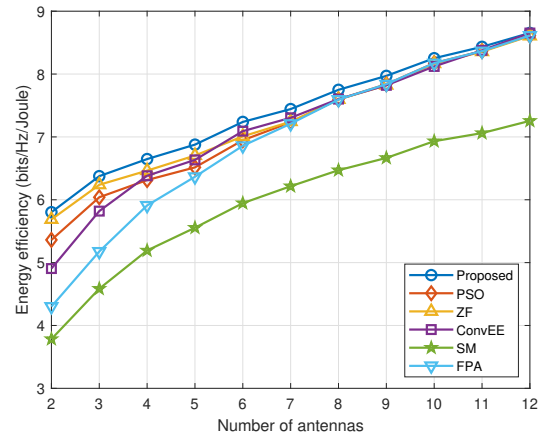


Fig. 13: EE performance versus the number of antennas.

performance among them. In addition, the performance gap between our proposed algorithm and the ConvEE benchmark decreases with T , due to the less significant effects of mechanical power consumption. However, their performance gap amounts to 1.5 bps/Hz/Joule as $T = 0.05$ s. It is also observed that the performance gap between our proposed algorithm and the FPA benchmark increases with T due to the enlarged data transmission time. The ZF benchmark is also observed to outperform the FPA benchmark when $T > 0.1$ s.

Lastly, we plot in Fig. 13 the EE performance versus the number of antennas, i.e., N . It is observed that the performance of all considered schemes increases with N , and our proposed algorithm consistently yields a higher EE performance compared to the other schemes, especially for small values of N . For example, when $N = 2$, the proposed scheme can yield an EE improvement over the ConvEE and SM benchmarks by 0.9 bps/Hz/Joule and 1.6 bps/Hz/Joule, respectively. However, the performance advantage of our proposed scheme diminishes as N increases, owing to less flexible antenna repositioning given a finite antenna movement region. This also reduces the total mechanical power consumption and leads to a smaller performance gap between the ConvEE scheme and our proposed algorithm.

VI. CONCLUSIONS AND FUTURE WORK

In this paper, we investigated an EE maximization problem for a stepper motor-driven multi-MA system. First, we developed a fundamental power consumption model for stepper motor-driven MAs based on electric motor theory. Based on this model, we formulated an EE maximization problem by jointly optimizing the MAs' destination positions, moving speed, and the BS's transmit precoding matrix, subject to the inter-MA collision avoidance constraints in their movement. To address this challenging optimization problem, we reveal that the inter-MA collision avoidance constraints can be safely relaxed and all MAs should move at their maximum velocity to maximize the EE. For the remaining BS precoding and MA destination position optimization problem, we proposed a two-layer optimization framework and an AO algorithm to solve it in the single- and multi-user scenarios, respectively.

Numerical results are provided to show the efficacy of our proposed algorithms in boosting the EE by properly balancing the rate performance and overall energy consumption. The main takeaways are summarized as follows. First, compared to the conventional FPA scheme, our proposed algorithm can explore more spatial diversity to improve the EE, especially in the low transmit power regime. Second, compared to the SM scheme, our proposed algorithm can avoid long-range MA movement that incurs substantial energy consumption and degrades EE. Third, unlike conventional EE maximization, rate maximization may only achieve suboptimal performance even in the low transmit power regime. Fourth, conventional EE maximization without accounting for mechanical energy consumption can lead to a significant EE loss in the cases of low channel coherence time, large antenna movement region, and small BS antenna number. Last but not least, the EE performance gain by MAs becomes less pronounced in the multi-user scenario compared to the single-user scenario, which is consistent with the observations made from achievable rate maximization with MAs [19], [25], [26], [34].

This paper can be extended to various directions as future work. First, it would be interesting to investigate the EE maximization for a more general two-dimensional (2D) planar array, which introduces additional spatial degrees of freedom but more challenging collision avoidance and moving trajectory design. Second, this paper assumes that each MA is driven via a dedicated stepper motor. It is worthy of studying the EE characterization and maximization under other MA architectures, such as cross-linked MAs, 6DMAs with antenna rotation, array-level MAs, extremely large MAs, among others. Third, the EE maximization under other system setups can also be studied by accounting for mechanical power consumption, such as physical-layer security, ISAC, mobile computing, and so on.

APPENDIX A PROOF OF PROPOSITION 1

Let $\mathbf{x} = [x_1, x_2, \dots, x_N]^T \in \mathbb{R}^{N \times 1}$ and $\mathbf{W} = [\mathbf{w}_1, \mathbf{w}_2, \dots, \mathbf{w}_K] \in \mathbb{C}^{N \times K}$ denote the optimized DPV and transmit precoding matrix without the collision-avoidance constraints in (6), respectively. We sort \mathbf{x} in an ascending order as $x_{q_1} < x_{q_2} < \dots < x_{q_N}$ with permutation indices $q_n \in \mathcal{N}$.

Then, we renumber \mathbf{x} and \mathbf{W} as $x_n = x_{q_n}$ and $\mathbf{w}_n = \mathbf{w}_{q_n}$, $n \in \mathcal{N}$, respectively. It has been proven in [46, **Theorem 1**] that the resulting trajectory from the CPV to the DPV \mathbf{x} is collision-free.

Let $\tau_n = \frac{|x_n - x_n^0|}{v}$ and $\tau'_n = \frac{|x_{q_n} - x_n^0|}{v}$ denote the movement delay of the n -th MA before/after the above renumbering, respectively. Next, we prove that this renumbering will not decrease the EE performance. Specifically, we rewrite the expression of EE in (13) into a more tractable form as

$$\begin{aligned} \text{EE}(\mathbf{W}, \mathbf{x}, v) &= \frac{(T - \tau) \sum_{k=1}^K R_k(\mathbf{W}, \mathbf{x})}{E_{\text{total}}(\mathbf{W}, \mathbf{x}, v)} \\ &= \frac{(T - \tau) \sum_{k=1}^K R_k(\mathbf{W}, \mathbf{x})}{\sum_{n=1}^N \tau_n P_M(v) + (T - \tau) P_D(\mathbf{W})} \\ &= \frac{\sum_{k=1}^K R_k(\mathbf{W}, \mathbf{x})}{P_M(v) \frac{\sum_{n=1}^N \tau_n}{T - \tau} + P_D(\mathbf{W})}. \end{aligned} \quad (39)$$

It is straightforward to see that the renumbering procedure does not affect the values of the sum-rate $\sum_{k=1}^K R_k(\mathbf{W}, \mathbf{x})$, the total transmit power $P_D(\mathbf{W})$, and the power consumption for the MA driver $P_M(v)$. In addition, as shown in [46, **Theorem 1**], the maximum delay after the renumbering is no greater than that before the renumbering, i.e.,

$$\tau' = \max_{n \in \mathcal{N}} \tau'_n \leq \tau = \max_{n \in \mathcal{N}} \tau_n, \quad (40)$$

or equivalently, $T - \tau' \geq T - \tau$. Hence, if

$$\sum_{n=1}^N \tau'_n \leq \sum_{n=1}^N \tau_n, \quad (41)$$

then the EE performance after the renumbering must be no worse than that before the renumbering. To prove (41), we present the following lemma.

Lemma 1: Consider four arbitrary positive numbers a, b, c , and d , with $a < b$ and $c < d$. Then, we have

$$|a - c| + |b - d| < |a - d| + |b - c|. \quad (42)$$

Lemma 1 can be proven readily by enumerating all possible relationships among the four numbers. Then, given the DPV $\mathbf{x} = [x_1, x_2, \dots, x_N]$, we define a pair (i, j) as a *reverse pair* if $i < j$ but $x_i > x_j$, $i, j \in \mathcal{N}$. It is evident to see that if there is no reverse pair for the DPV \mathbf{x} , then the equality in (41) should hold. If there exists at least one reverse pair (i, j) , by applying Lemma 1, we have

$$\begin{aligned} \sum_{n=1}^N \tau_n &= \sum_{m \neq i, j} \tau_m + \frac{|x_i^0 - x_j|}{v} + \frac{|x_j^0 - x_i|}{v} \\ &> \sum_{m \neq i, j} \tau_m + \frac{|x_i^0 - x_i|}{v} + \frac{|x_j^0 - x_j|}{v}, \end{aligned} \quad (43)$$

which indicates that the total delay can be reduced by swapping the indices i and j . Since the number of reverse pairs is finite, the swapping process in (43) can be repeated for any all remaining reverse pairs until no reverse pairs remain, which leads to $x_n = x_{q_n}$, $\forall n \in \mathcal{N}$. Hence, the inequality in (41) is established. Based on the above, (41) must hold after the renumbering. Hence, Proposition 1 is proved.

REFERENCES

- [1] X. Wei, W. Mei, X. Huang, Z. Chen, and B. Ning, "Mechanical power modeling and energy efficiency maximization for movable antenna systems," 2025. [Online]. Available: <https://arxiv.org/pdf/2505.05914>
- [2] E. G. Larsson, O. Edfors, F. Tufvesson, and T. L. Marzetta, "Massive MIMO for next generation wireless systems," *IEEE Commun. Mag.*, vol. 52, no. 2, pp. 186–195, Feb. 2014.
- [3] Z. Wang *et al.*, "A tutorial on extremely large-scale MIMO for 6G: Fundamentals, signal processing, and applications," *IEEE Commun. Surveys Tuts.*, vol. 26, no. 3, pp. 1560–1605, 2024.
- [4] L. Zhu, W. Ma, and R. Zhang, "Movable antennas for wireless communication: Opportunities and challenges," *IEEE Commun. Mag.*, vol. 62, no. 6, pp. 114–120, Jun. 2024.
- [5] J. Zheng, J. Zhang, H. Du, D. Niyato, S. Sun, B. Ai, and K. B. Letaief, "Flexible-position MIMO for wireless communications: Fundamentals, challenges, and future directions," *IEEE Wireless Commun.*, vol. 31, no. 5, pp. 18–26, Oct. 2024.
- [6] W. K. New *et al.*, "A tutorial on fluid antenna system for 6G networks: Encompassing communication theory, optimization methods and hardware designs," *IEEE Commun. Surveys Tuts.*, vol. 27, no. 4, pp. 2325–2377, Aug. 2025.
- [7] L. Zhu, W. Ma, W. Mei, Y. Zeng, Q. Wu, B. Ning, Z. Xiao, X. Shao, J. Zhang, and R. Zhang, "A tutorial on movable antennas for wireless networks," *IEEE Commun. Surveys Tuts.*, 2025, early access.
- [8] L. Zhu, W. Ma, and R. Zhang, "Modeling and performance analysis for movable antenna enabled wireless communications," *IEEE Trans. Wireless Commun.*, vol. 23, no. 6, pp. 6234–6250, Jun. 2024.
- [9] B. Ning *et al.*, "Movable antenna-enhanced wireless communications: General architectures and implementation methods," *IEEE Wireless Commun.*, 2025, early access.
- [10] W. Ma, L. Zhu, and R. Zhang, "MIMO capacity characterization for movable antenna systems," *IEEE Trans. Wireless Commun.*, vol. 23, no. 4, pp. 3392–3407, Sep. 2024.
- [11] L. Zhu, W. Ma, and R. Zhang, "Movable-antenna array enhanced beamforming: Achieving full array gain with null steering," *IEEE Commun. Lett.*, vol. 27, no. 12, pp. 3340–3344, Dec. 2023.
- [12] W. Ma, L. Zhu, and R. Zhang, "Multi-beam forming with movable-antenna array," *IEEE Commun. Lett.*, vol. 28, no. 3, pp. 697–701, Mar. 2024.
- [13] K. Liu, X. Wei, W. Mei, X. Wei, B. Ning, and Z. Chen, "Movable antennas for the multicasting: Grating-lobe analysis and position optimization," *Sci. China Inf. Sci.*, vol. 68, no. 10, pp. 209 302:1–209 302:2, Oct. 2025.
- [14] D. Wang, W. Mei, B. Ning, Z. Chen, and R. Zhang, "Movable antenna enhanced wide-beam coverage: Joint antenna position and beamforming optimization," *IEEE Trans. Wireless Commun.*, pp. 1–1, 2025, early access.
- [15] W. Mei, X. Wei, Y. Liu, B. Ning, and Z. Chen, "Movable-antenna position optimization for physical-layer security via discrete sampling," in *Proc. IEEE Global Commun. Conf.*, Cape Town, South Africa, Dec. 2024, pp. 4739–4744.
- [16] J. Tang, C. Pan, Y. Zhang, H. Ren, and K. Wang, "Secure MIMO communication relying on movable antennas," *IEEE Trans. Commun.*, vol. 73, no. 4, pp. 2159–2175, Apr. 2025.
- [17] X. Shen, X. Wei, W. Mei, Z. Chen, J. Fang, and B. Ning, "Movable-antenna-enhanced physical-layer service integration: Performance analysis and optimization," *IEEE Wireless Commun. Lett.*, pp. 1–1, 2025, early access.
- [18] W. Mei, X. Wei, B. Ning, Z. Chen, and R. Zhang, "Movable-antenna position optimization: A graph-based approach," *IEEE Wireless Commun. Lett.*, vol. 13, no. 7, pp. 1853–1857, Jul. 2024.
- [19] L. Zhu, W. Ma, B. Ning, and R. Zhang, "Movable-antenna enhanced multiuser communication via antenna position optimization," *IEEE Trans. Wireless Commun.*, vol. 23, no. 7, pp. 7214–7229, Jul. 2024.
- [20] H. Ma, W. Mei, X. Wei, B. Ning, and Z. Chen, "Robust movable-antenna position optimization with imperfect CSI for MISO systems," *IEEE Commun. Lett.*, vol. 29, no. 7, pp. 1594–1598, Jul. 2025.
- [21] X. Wei, W. Mei, D. Wang, B. Ning, and Z. Chen, "Joint beamforming and antenna position optimization for movable antenna-assisted spectrum sharing," *IEEE Wireless Commun. Lett.*, vol. 13, no. 9, pp. 2502–2506, Sep. 2024.
- [22] N. Li, W. Mei, P. Wu, B. Ning, and L. Zhu, "Movable antenna enhanced DF and AF relaying systems: Performance analysis and optimization," *IEEE Trans. Commun.*, pp. 1–1, 2025, early access.
- [23] N. Li, P. Wu, B. Ning, and L. Zhu, "Sum rate maximization for movable antenna enabled uplink NOMA," *IEEE Wireless Commun. Lett.*, vol. 13, no. 8, pp. 2140–2144, Aug. 2024.
- [24] N. Li, P. Wu, L. Zhu, W. Mei, B. Ning, and D. W. K. Ng, "Sum-rate maximization for movable-antenna array enhanced downlink NOMA systems," 2025. [Online]. Available: <https://arxiv.org/pdf/2507.15555>
- [25] X. Wei, W. Mei, Q. Wu, Q. Jia, B. Ning, Z. Chen, and J. Fang, "Movable antennas meet intelligent reflecting surface: Friends or foes?" *IEEE Trans. Commun.*, pp. 1–1, 2025, early access.
- [26] B. Zhang, K. Xu, X. Xia, G. Hu, C. Wei, C. Li, and K. Cheng, "Sum-rate enhancement for RIS-assisted movable antenna systems: Joint transmit beamforming, reflecting design, and antenna positioning," *IEEE Trans. Veh. Technol.*, vol. 74, no. 3, pp. 4376–4392, Mar. 2025.
- [27] W. Ma, L. Zhu, and R. Zhang, "Movable antenna enhanced wireless sensing via antenna position optimization," *IEEE Trans. Wireless Commun.*, vol. 23, no. 11, pp. 16 575–16 589, Nov. 2024.
- [28] Y. Wang, W. Mei, X. Wei, B. Ning, and Z. Chen, "Antenna position optimization for movable antenna-empowered near-field sensing," in *Proc. IEEE Int. Conf. Commun. Workshops*, 2025, pp. 324–329.
- [29] W. Lyu, S. Yang, Y. Xiu, Z. Zhang, C. Assi, and C. Yuen, "Movable antenna enabled integrated sensing and communication," *IEEE Trans. Wireless Commun.*, vol. 24, no. 4, pp. 2862–2875, Apr. 2025.
- [30] L. Chen, M.-M. Zhao, M.-J. Zhao, and R. Zhang, "Antenna position and beamforming optimization for movable antenna enabled ISAC: Optimal solutions and efficient algorithms," *IEEE Trans. Signal Process.*, pp. 1–16, 2025, early access.
- [31] X. Shao and R. Zhang, "6DMA enhanced wireless network with flexible antenna position and rotation: Opportunities and challenges," *IEEE Commun. Mag.*, vol. 63, no. 4, pp. 121–128, Apr. 2025.
- [32] Z. Ding, R. Schober, and H. Vincent Poor, "Flexible-antenna systems: A pinching-antenna perspective," *IEEE Trans. Commun.*, pp. 1–1, 2025, early access.
- [33] X. Chen, B. Feng, Y. Wu, and W. Zhang, "Energy efficiency maximization for movable antenna-enhanced system based on statistical CSI," 2025. [Online]. Available: <https://arxiv.org/pdf/2501.10694>
- [34] Y. Wu, D. Xu, D. W. K. Ng, W. Gerstacker, and R. Schober, "Globally optimal movable antenna-enabled multiuser communication: Discrete antenna positioning, power consumption, and imperfect CSI," *IEEE Trans. Commun.*, pp. 1–1, 2025, early access.
- [35] J. Ding, Z. Zhou, L. Zhu, Y. Zhao, B. Jiao, and R. Zhang, "Energy efficiency maximization for movable antenna communication systems," *IEEE Trans. Wireless Commun.*, pp. 1–1, 2025, early access.
- [36] J. Xu and L. Qiu, "Energy efficiency optimization for MIMO broadcast channels," *IEEE Trans. Wireless Commun.*, vol. 12, no. 2, pp. 690–701, Feb. 2013.
- [37] P. Acarnley, *Stepping motors: A guide to theory and practice*. Iet, 2002, no. 63.
- [38] W. Ma, L. Zhu, and R. Zhang, "Compressed sensing based channel estimation for movable antenna communications," *IEEE Commun. Lett.*, vol. 27, no. 10, pp. 2747–2751, Oct. 2023.
- [39] R. Zhang, L. Cheng, W. Zhang, X. Guan, Y. Cai, W. Wu, and R. Zhang, "Channel estimation for movable-antenna MIMO systems via tensor decomposition," *IEEE Wireless Commun. Lett.*, vol. 13, no. 11, pp. 3089–3093, Nov. 2024.
- [40] Y. Huang, W. Mei, X. Wei, Z. Chen, and B. Ning, "CNN-based channel map estimation for movable antenna systems," in *Proc. IEEE 26th Int. IEEE Int. Wkshps. Sig. Proc. Adv. Wireless Commun. (SPAWC)*, 2025, pp. 1–5.
- [41] Z. Xiao, X. Pi, L. Zhu, X.-G. Xia, and R. Zhang, "Multiuser communications with movable-antenna base station: Joint antenna positioning, receive combining, and power control," *IEEE Trans. Wireless Commun.*, vol. 23, no. 12, pp. 19 744–19 759, Dec. 2024.
- [42] K.-Y. Wang, A. M.-C. So, T.-H. Chang, W.-K. Ma, and C.-Y. Chi, "Outage constrained robust transmit optimization for multiuser MISO downlinks: Tractable approximations by conic optimization," *IEEE Trans. Signal Process.*, vol. 62, no. 21, pp. 5690–5705, Nov. 2014.
- [43] Faulhaber, "Stepper Motors, Series AM2224," [Online], <https://www.faulhaber.com/en/products/series/am2224>.
- [44] Q. Shi, M. Razaviyayn, Z.-Q. Luo, and C. He, "An iteratively weighted MMSE approach to distributed sum-utility maximization for a MIMO interfering broadcast channel," *IEEE Trans. Signal Process.*, vol. 59, no. 9, pp. 4331–4340, Sep. 2011.
- [45] C. Huang, A. Zappone, G. C. Alexandropoulos, M. Debbah, and C. Yuen, "Reconfigurable intelligent surfaces for energy efficiency in wireless communication," *IEEE Trans. Wireless Commun.*, vol. 18, no. 8, pp. 4157–4170, Aug. 2019.
- [46] Q. Li, W. Mei, R. Zhang, and B. Ning, "Trajectory optimization for minimizing movement delay in movable antenna systems," 2025. [Online]. Available: <https://www.techrxiv.org/doi/full/10.36227/techrxiv.174952511.11885387>